Implementation of PT symmetric devices using plasmonics: principle and applications

Henri Benisty, Aloyse Degiron, Anatole Lupu, André de Lustrac, Sébastien Chenais, Sébastien Forget, Mondher Besbes, Grégory Barbillon, Aurélien Bruyant, Sylvain Blaize, et al.

Implementation of PT symmetric devices using plasmonics: principle and applications

Henri Benisty,[1,*] Aloyse Degiron,[2] Anatole Lupu,[2] André De Lustrac,[2] Sébastien Chénais,[3] Sébastien Forget,[3] Mondher Besbes,[1] Grégory Barbillon,[1] Aurélien Bruyant,[4] Sylvain Blaize,[4] and Gilles Lérondel[4]

[1]*Laboratoire Charles Fabry de l'Institut d'Optique, CNRS, Univ. Paris-Sud, Campus Polytechnique, RD 128, 91127 Palaiseau Cedex, France*
[2]*Institut d'Électronique Fondamentale, UMR 8622 du CNRS, Université Paris-Sud, Bât. 220, 91405 Orsay Cedex, France*
[3]*Laboratoire de Physique des Lasers, UMR 7538, Université Paris, 13/CNRS, 93430 Villetaneuse, France*
[4]*Laboratoire de Nanotechnologie et d'Instrumentation Optique, Institut Charles Delaunay, CNRS-FRE 2848, Université de Technologie de Troyes, BP 2060, 10010 Troyes, France*
*henri.benisty@institutoptique.fr

Abstract: The so-called PT symmetric devices, which feature $\varepsilon_{(-x)} = \varepsilon_{(x)}^*$ associated with parity-time symmetry, incorporate both gain and loss and can present a singular eigenvalue behaviour around a critical transition point. The scheme, typically based on co-directional coupled waveguides, is here transposed to the case of variable gain on one arm with fixed losses on the other arm. In this configuration, the scheme exploits the full potential of plasmonics by making a beneficial use of their losses to attain a critical regime that makes switching possible with much lowered gain excursions. Practical implementations are discussed based on existing attempts to elaborate coupled waveguide in plasmonics, and based also on the recently proposed hybrid plasmonics waveguide structure with a small low-index gap, the PIROW (Plasmonic Inverse-Rib Optical Waveguide).

References and links

1. D. J. Bergman and M. I. Stockman, "Surface plasmon amplification by stimulated emission of radiation: quantum generation of coherent surface plasmons in nanosystems," Phys. Rev. Lett. **90**(2), 027402 (2003).
2. R. F. Oulton, V. J. Sorger, T. Zentgraf, R.-M. Ma, C. Gladden, L. Dai, G. Bartal, and X. Zhang, "Plasmon lasers at deep subwavelength scale," Nature **461**(7264), 629–632 (2009).
3. I. De Leon and P. Berini, "Amplification of long-range surface plasmons by a dipolar gain medium," Nat. Photonics **4**(6), 382–387 (2010).
4. M. C. Gather, K. Meerholz, N. Danz, and K. Leosson, "Net optical gain in a plasmonic waveguide embedded in a fluorescent polymer," Nat. Photonics **4**(7), 457–461 (2010).
5. S. Klaiman, U. Günther, and N. Moiseyev, "Visualization of branch points in PT-symmetric waveguides," Phys. Rev. Lett. **101**(8), 080402 (2008).
6. T. Kottos, "Broken symmetry makes light work," Nat. Phys. **6**(3), 166–167 (2010).
7. K. G. Makris, R. El-Ganainy, D. N. Christodoulides, and Z. H. Musslimani, "Beam dynamics in PT symmetric optical lattices," Phys. Rev. Lett. **100**(10), 103904 (2008).
8. C. E. Rüter, K. G. Makris, R. El-Ganainy, D. N. Christodoulides, M. Segev, and D. Kip, "Observation of parity–time symmetry in optics," Nat. Phys. **6**(3), 192–195 (2010).
9. S. Klaiman and L. S. Cederbaum, "Non-Hermitian Hamiltonians with space-time symmetry," Phys. Rev. A **78**(6), 062113 (2008).
10. J. Čtyroký, V. Kuzmiak, and S. Eyderman, "Waveguide structures with antisymmetric gain/loss profile," Opt. Express **18**(21), 21585–21593 (2010).
11. H.-P. Nolting, G. Sztefka, M. Grawert, and J. Čtyroký, in *Integrated Photonics Research*, Vol. 6 of 1996 OSA Technical Digest Series (Optical Society of America, 1996), paper IMD5.
12. M. Kulishov, J. M. Laniel, N. Bélanger, J. Azaña, and D. V. Plant, "Nonreciprocal waveguide Bragg gratings," Opt. Express **13**(8), 3068–3078 (2005).
13. M. Kulishov, J. M. Laniel, N. Bélanger, and D. V. Plant, "Trapping light in a ring resonator using a grating-assisted coupler with asymmetric transmission," Opt. Express **13**(9), 3567–3578 (2005).

14. R. F. Oulton, V. J. Sorger, D. A. Genov, D. F. P. Pile, and X. Zhang, "A hybrid plasmonic waveguide for subwavelength confinement and long-range propagation," Nat. Photonics **2**(8), 496–500 (2008).
15. M. P. Nezhad, K. Tetz, and Y. Fainman, "Gain assisted propagation of surface plasmon polaritons on planar metallic waveguides," Opt. Express **12**(17), 4072–4079 (2004).
16. M. A. Noginov, G. Zhu, A. M. Belgrave, R. Bakker, V. M. Shalaev, E. E. Narimanov, S. Stout, E. Herz, T. Suteewong, and U. Wiesner, "Demonstration of a spaser-based nanolaser," Nature **460**(7259), 1110–1112 (2009).
17. R.-M. Ma, R. F. Oulton, V. J. Sorger, G. Bartal, and X. Zhang, "Room-temperature sub-diffraction-limited plasmon laser by total internal reflection," Nat. Mater. **10**(2), 110–113 (2011).
18. H. Benisty and M. Besbes, "Plasmonic inverse rib waveguiding for tight confinement and smooth interface definition," J. Appl. Phys. **108**(6), 063108 (2010).
19. J. Grandidier, S. Massenot, G. des Francs, A. Bouhelier, J.-C. Weeber, L. Markey, A. Dereux, J. Renger, M. González, and R. Quidant, "Dielectric-loaded surface plasmon polariton waveguides: figures of merit and mode characterization by image and Fourier plane leakage microscopy," Phys. Rev. B **78**(24), 245419 (2008).
20. A. Guo, G. J. Salamo, M. Volatier-Ravat, V. Aimez, G. A. Siviloglou, and D. N. Christodoulides, "Observation of PT-symmetry breaking in complex optical potentials," Phys. Rev. Lett. **103**(9), 093902 (2009).
21. H. Ramezani, T. Kottos, R. El-Ganainy, and D. N. Christodoulides, "Unidirectional nonlinear PT-symmetric optical structures," Phys. Rev. A **82**(4), 043803 (2010).
22. P. Berini, "Plasmon-polariton waves guided by thin lossy metal films of finite width: Bound modes of symmetric structures," Phys. Rev. B **61**(15), 10484–10503 (2000).
23. P. Berini, "Plasmon-polariton waves guided by thin lossy metal films of finite width: Bound modes of asymmetric structures," Phys. Rev. B **63**(12), 125417 (2001).
24. A. Boltasseva, V. S. Volkov, R. B. Nielsen, E. Moreno, S. G. Rodrigo, and S. I. Bozhevolnyi, "Triangular metal wedges for subwavelength plasmon-polariton guiding at telecom wavelengths," Opt. Express **16**(8), 5252–5260 (2008).
25. T. Holmgaard, J. Gosciniak, and S. I. Bozhevolnyi, "Long-range dielectric-loaded surface plasmon-polariton waveguides," Opt. Express **18**(22), 23009–23015 (2010).
26. C. Jeppesen, R. B. Nielsen, A. Boltasseva, S. Xiao, N. A. Mortensen, and A. Kristensen, "Thin film Ag superlens towards lab-on-a-chip integration," Opt. Express **17**(25), 22543–22552 (2009).
27. V. Z. Zayats, I. I. Smolyaninov, and A. A. Maradudin, "Nano-optics of surface plasmon polaritons," Phys. Rep. **408**(3–4), 131–314 (2005).
28. K. Leosson, T. Nikolajsen, A. Boltasseva, and S. I. Bozhevolnyi, "Long-range surface plasmon polariton nanowire waveguides for device applications," Opt. Express **14**(1), 314–319 (2006).
29. M. A. Noginov, V. A. Podolskiy, G. Zhu, M. Mayy, M. Bahoura, J. A. Adegoke, B. A. Ritzo, and K. Reynolds, "Compensation of loss in propagating surface plasmon polariton by gain in adjacent dielectric medium," Opt. Express **16**(2), 1385–1392 (2008).
30. C. Delacour, S. Blaize, P. Grosse, J. M. Fedeli, A. Bruyant, R. Salas-Montiel, G. Lerondel, and A. Chelnokov, "Efficient directional coupling between silicon and copper plasmonic nanoslot waveguides: toward metal-oxide-silicon nanophotonics," Nano Lett. **10**(8), 2922–2926 (2010).
31. A. Degiron, S. Y. Cho, T. Tyler, N. M. Jokerst, and D. R. Smith, "Directional coupling between dielectric and long-range plasmon waveguides," N. J. Phys. **11**(1), 015002 (2009).
32. N. C. Giebink and S. R. Forrest, "Temporal response of optically pumped organic semiconductor lasers and its implication for reaching threshold under electrical excitation," Phys. Rev. B **79**(7), 073302 (2009).
33. R. Harbers, P. Strasser, D. Caimi, R. F. Mahrt, N. Moll, B. J. Offrein, D. Erni, W. Bächtold, and U. Scherf, "Enhanced feedback in organic photonic-crystal lasers," Appl. Phys. Lett. **87**(15), 151121 (2005).
34. H. Rabbani-Haghighi, S. Forget, S. Chénais, A. Siove, M.-C. Castex, and E. Ishow, "Laser operation in nondoped thin films made of a small-molecule organic red-emitter," Appl. Phys. Lett. **95**(3), 033305 (2009).
35. G. Wegmann, B. Schweitzer, D. Hertel, H. Giessen, M. Oestreich, U. Scherf, K. Müllen, and R. F. Mahrt, "The dynamics of gain-narrowing in a ladder-type [pi]-conjugated polymer," Chem. Phys. Lett. **312**(5–6), 376–384 (1999).
36. T. Virgili, D. G. Lidzey, D. D. C. Bradley, G. Cerullo, S. Stagira, and S. De Silvestri, "An ultrafast spectroscopy study of stimulated emission in poly(9,9-dioctylfluorene) films and microcavities," Appl. Phys. Lett. **74**(19), 2767–2769 (1999).
37. K. L. Shaklee and R. F. Leheny, "Direct determination of optical gain in semiconductor crystals," Appl. Phys. Lett. **18**(11), 475–477 (1971).
38. L. Pavesi, L. Dal Negro, C. Mazzoleni, G. Franzò, and F. Priolo, "Optical gain in silicon nanocrystals," Nature **408**(6811), 440–444 (2000).
39. L. Dal Negro, P. Bettotti, M. Cazzanelli, D. Pacifici, and L. Pavesi, "Applicability conditions and experimental analysis of the variable stripe length method for gain measurements," Opt. Commun. **229**(1-6), 337–348 (2004).
40. H. Rabbani-Haghighi, S. Forget, S. Chénais, and A. Siove, "Highly efficient, diffraction-limited laser emission from a vertical external-cavity surface-emitting organic laser," Opt. Lett. **35**(12), 1968–1970 (2010).
41. A. Costela, O. García, L. Cerdán, I. García-Moreno, and R. Sastre, "Amplified spontaneous emission and optical gain measurements from pyrromethene 567--doped polymer waveguides and quasi-waveguides," Opt. Express **16**(10), 7023–7036 (2008).
42. M. D. McGehee, R. Gupta, S. Veenstra, E. K. Miller, M. A. Diaz-Garcia, and A. J. Heeger, "Amplified spontaneous emission from photopumped films of a conjugated polymer," Phys. Rev. B **58**(11), 7035–7039 (1998).

1. Introduction

Including gain in plasmonic systems and compensating their inherent Joule losses is a privileged route to make plasmonic technologies viable into nanodevices [1]. Recent years have witnessed the first "plasmon lasers" or "spasers" [2], as well as several noteworthy gain measurements in systems that combine gain materials from organics rare earths or semiconductors [3,4] with plasmonic guides of various types.

We develop here the combination of gain and plasmonics within the framework of the recently proposed "PT symmetric devices", whose dielectric landscape $\varepsilon(x)$ features $\varepsilon_{(-x)} = \varepsilon_{(x)}^*$, that is a PT symmetric combination of gain and loss, with a spatial plane symmetry, say σ_x, exchanging "gainy" parts and "lossy" ones [5–8]. Practically, a set of coupled waveguides, one with gain and the other with loss in a symmetric amount is an embodiment of such a device [5,9,10] and has interested the integrated optics community since the 90s [11]. Grating variants, whereby the symmetry plane involved is normal to the guide axis [12,13], are of high interest but more difficult to implement and not considered here. We show that their essential features, and notably a singular *critical behaviour* around their so-called exceptional point, can be retained with proper design when using plasmonics, even if (i) the above relation is obeyed only around a specific working point due to the fixed losses of metals and (ii) the two guides have a distinct material support and a distinct field structure. The interest of a critical behaviour is to enhance the modulation capability of such devices, meaning that a large output signal change is induced by a modest swing in control parameter, e.g., gain, yielding a transduction coefficient larger than in a single non PT symmetric device. We shall later refer to this positive effect as a "Singular Eigenvalue Behaviour" (SEB), denoting that we use not only the exceptional point but also its vicinity. Possible applications include optical memories [8,13].

From our own gain analysis exposed later, we find it necessary to orient our choice toward hybrid dielectric-plasmonic waveguiding in order to achieve a still highly-confined guidance at a lower loss penalty. This strategy has been implemented for example by Oulton et al. [14] and has been the key of Berkeley's "spaser", a CdS nano-rod with strong band-to-band recombination near 500 nm, on top of a silver layer, separated by a thin low-index nanogap [2]. This structure is nearly deterministic, even though the rods are not yet elaborated nor positioned by a top-down method. A symmetrical proposal of a metallic ribbon near a gain-carrying dielectric slab was briefly discussed in the framework of direct loss compensation of a plasmonic mode by the adjacent dielectric system [15], but a high confinement effect was not specifically addressed, the spacing lower index layer being seen as a technical requirement when dealing with highly injected layers in semiconductors. The other spaser realisation by Noginov *et al.* [16] being clearly nondeterministic, it cannot presently be easily knitted with the PT symmetric approach into nanodevices, but further advances could trigger unheard combinations. Oulton's formal proposal [14] concern rods whose in-plane position is still random (or CdS flakes [17] that work at room temperature). The recent PIROW proposal (Plasmonics Inverse-Rib Optical Waveguide) [18] has pointed out a simple solution to hybrid waveguiding from proven lithography-etching techniques. We will discuss its applicability here, taking into account recent advances [3,4,19].

The paper is organized as follows: in the next Sec.2, we describe the essential physics of true PT symmetric coupled waveguides, and of adequately designed plasmonics implementations with fixed losses, that retain notably the same local SEB pattern,. In Sec.3 we discuss the implementation of PT-symmetric devices exhibiting the desired SEB from the toolbox of dielectric and plasmonics. We first review the essential coupled waveguide approaches in plasmonics. We envision notably the use of long-Range Surface plasmon polariton (LRSPP) waveguides, based on thin metal layers. We describe an implementation that should ensure the criteria for exhibiting SEB. We carry out a similar work for the more confined PIROW waveguide, assuming a confined dielectric gain-carrying waveguide as an ingredient. Finally, in Sec.4, we detail current knowledge on gain from organics, needed to operate in the visible or near-infrared, which is the most promising way towards incorporating

gain into cheap large-scale nanoplasmonic devices. We discuss why gains in the 100-500 cm^{-1} range can be targeted. The popular Variable Stripe Length (VSL) technique routinely enables assessing gains lower than 100 cm^{-1}, but it can be shown that there is a fair margin for higher gains with existing organic materials, favourable to miniature devices.

2. PT symmetric coupled waveguides and the plasmonic variant

Let us start with the model system exhibiting singular eigenvalue behaviour, shown in Fig. 1(a) below. Let us also briefly remind that the initial idea was to study operators with real eigenvalues but that are not Hermitian, hermiticity being a sufficient but not a necessary condition for obtaining real eigenvalues.
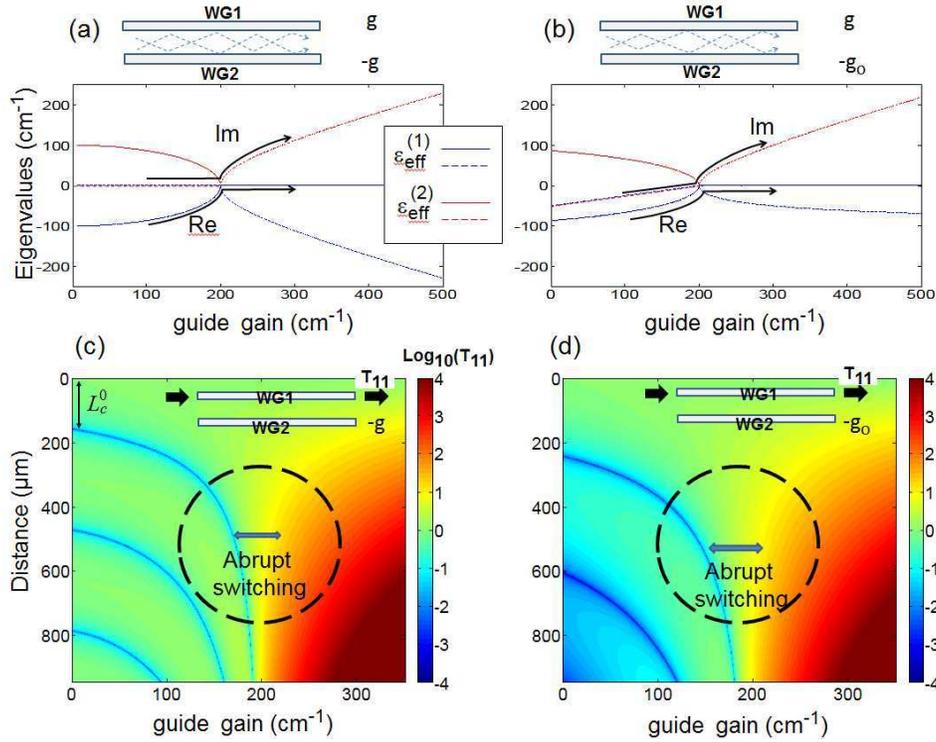

Fig. 1. Real parts (solid lines) and Imaginary parts (dashed line) of the two eigenvalues $\beta_{eff}^{(1)}$ and $\beta_{eff}^{(2)}$ (red and blue) of a coupled system; (a) for balanced gain and loss, the increase of material gain g brings the system through a "phase transition" point whereby the eigenvalues suddenly switch to the complex domain; (b) in a system with coupling adjusted to one arm's fixed losses $|-g_o|{\sim}\kappa$, the behaviour still exhibits a critical point. (c) Colour map of $\log_{10}(T_{11}(g_1))$, the bar transmission, in case (a), blue lines, T<<1, are the classical periodic zeros of coupled waveguides with supermode beating. The circle evidences the high sensitivity zone, a relative gain variation of 20%, brings >3 decades variation in transmission. (d) Colour map of $\log_{10}(T_{11}(g_1))$ for the fixed loss (i.e., plasmonics) case (b).

The reference model system for our purpose consists of a pair of parallel coupled waveguides (see e.g., [5,9]), one of them with gain **g,** the other with a symmetric loss, **-g.** This optical structure has a dielectric constant distribution $\varepsilon(x,y,z)$ that can be assimilated to a complex potential landscape obeying the essential SEB requirement $\varepsilon_{(-x)} = \varepsilon_{(x)}^{*}$: we have $\varepsilon = \varepsilon_1 + ig$ in waveguide WG1 and $\varepsilon = \varepsilon_1 - ig$ in waveguide WG2 (the actual spatial power gain is 2 Im($\varepsilon^{1/2}$) $\approx g/\varepsilon_1^{1/2}$). Propagation inside each isolated guide can be described by an effective dielectric

constant. To avoid useless notations, we use the same notation $\varepsilon \equiv \varepsilon_{\text{eff}} = \varepsilon_1 \pm ig$ as above. For a proper design, it suffices to conjugate these effective quantities; there is no explicit need to conjugate the whole landscape because we are interested in the PT symmetry only in a restricted phase space of the problem, the modes of the waveguides, and thus not all electromagnetic solutions.

In other words, the guided modes are singularities that "pick up" the radiation from the other guide at a single wavevector $k(\omega)$, somehow ignoring the details of the field structure in the other guide. The behaviour of the whole system can then be found with the coupled wave equations, assuming as an approximation that the proximity of the two waveguides translates into some real coupling constant κ.

We use a scalar version and denote the relevant field component by $\psi_1(z)$ in WG1 and $\psi_2(z)$ in WG2. By proper normalization of propagation constants, with κ denoting the coupling constant, the coupled mode equation reads:

$$i \frac{d}{dz} \begin{pmatrix} \psi_1 \\ \psi_2 \end{pmatrix} = \begin{pmatrix} \beta_1 + ig_1/2 & \kappa \\ \kappa & \beta_1 - ig_1/2 \end{pmatrix} \begin{pmatrix} \psi_1 \\ \psi_2 \end{pmatrix} \tag{1}$$

where the diagonal terms, given by $(\beta_1 \pm ig_1/2)^2 = (\varepsilon_1 \pm ig)(\omega/c)^2$, are the forward propagation constants of uncoupled waveguide electromagnetic modes at frequency $\omega/2\pi = c/\lambda$ for vacuum wavelength λ. Power gain/loss per unit length is given by $\pm g_1$. It is easy to solve for Eq. (1) across a length L in the form of a transmission matrix

$$\begin{pmatrix} \psi_1 \\ \psi_2 \end{pmatrix}_{z=L} = P^{-1} \exp(DL) P \begin{pmatrix} \psi_1 \\ \psi_2 \end{pmatrix}_{z=0} = \begin{pmatrix} T_{11} & T_{12} \\ T_{21} & T_{22} \end{pmatrix} \begin{pmatrix} \psi_1 \\ \psi_2 \end{pmatrix}_{z=0} \tag{2}$$

where D is the diagonal matrix of eigenvalues of Eq. (1) right hand matrix within a factor i, and P the matrix of eigenvectors. For numerics and classical difficulties associated with large exponentials, one may recourse to a scattering matrix version, not used here though.

The initial motivations of the SEB phenomena were concerned with the two extreme behaviours of the system appearing in Fig. 1(a) done for $\kappa = 100\ cm^{-1}$:

At low gain, coupling is privileged over gain/loss, therefore, in spite of the non Hermitian nature of the operator in Eq. (1), its supermodes have *real* opposite eigenvalues. The system thus retains the very classical behaviour of a directional coupler with energy sloshing from one arm to the other. The beating length increases as gain is increased. Jumping over the singularity, at high gain, we have two opposite *imaginary* eigenvalues. At the exit of the system $z = L$, only the eigenvalue with gain will survive and thus, the corresponding eigenvector is exclusively observed. In practice, the system now preferentially routes the input to the output of the gain waveguide WG1. This is obvious if the input is WG1, i.e. if we look at T_{11}, but more strikingly, it shall feed the same exit WG1 even if the *lossy* waveguide WG2 is first excited, with T_{12} being comparable to T_{11}. Such behaviour makes this system equivalent to a nonsymmetrical combiner. This behaviour was found not only for co-directional coupling, but also for contradirectional coupling in a single guide but with a grating and a "nested" PT symmetry at the scale of the grating period ($\sim \lambda/2$) [12,13].
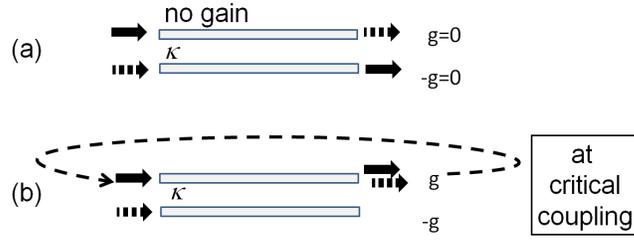
Fig. 2. Classical coupler behaviour (a) and (b) "unidirectional" behaviour with gain or loss above the symmetry-breaking point: inputs on both ports lead to the same output. The thin dashed line shows how feedback turns the system into a memory.

Of clear interest is the SEB around the singular point with abrupt derivatives, situated at $g_1 / 2 = \kappa$. Near this singular point, a small modulation of gain/loss results in a large change of supermodes' propagation. Such a point is tempting to exploit inside devices, to enhance the transduction coefficient of a modulator for instance. The reader may be familiar with similar transitions of eigenvalues for vacuum Rabi splitting (strong coupling), when the photon or the atom/exciton features increasing losses, but in this well-known case, the evolution lies only on the loss side; the splitting vanishes and weak coupling plainly arises. At variance with this scenario, the non-Hermitian behaviour in a gain-supporting system does lead to functionalities such as optical memories as described in Fig. 2, when a loop is implemented [13].

The map of Fig. 1(c) gives a color map of $T_{11}(g_1)$ as a function of gain and guide length (not guide separation). In this figure, the vertical cross-sections show the variation of T_{11} as a function of the propagating distance for a fixed amount of gain. For small gains, T_{11} has an oscillatory behaviour indicating that all the power is periodically transferred to the second waveguide by directional coupling. The beat length L_{beat}^0 is seen to diverge at the approach of the transition region, and then gain piles up in the channel (L_{beat}^0 is twice the coupling length for guide-to-guide transfer, $L_{\text{beat}}^0 = 2 L_c^0$). Of course, this simple model predicts large overall gains not far above the critical threshold without consideration of possible adverse effects such as saturation. A much more complete model would be needed to address the physics in these regions, where lasing could occur for instance and clamp the gain. We can postpone such studies because the SEB behavior that attracts our attention in this paper addresses the transition region located within the dashed circle of Fig. 1(c). In this region, and this is our main point, the model unambiguously suggests that a change in gain of modest magnitude (<20% of total gain) does result in a complete switching behaviour. Figure 1(c) indicates that this region with a high potential for switching exists for couplers with a total length L_{dev} roughly equal to 3 times the coupling length L_c^0 in the absence of gain.

Note also the relationship between beat length and decay(/gain) length *at the critical point*: the beat length of co-directional coupling is $L_{\text{beat}}^0 = \pi / \kappa = 2L_c^0$, and thus the decay length for loss $g_1^{\text{crit}} / 2 = \kappa$ is $L_d = (g_1^{\text{crit}})^{-1} = \kappa^{-1} / 2 = L_c^0 / \pi = L_{\text{beat}}^0 / 2\pi$. Therefore a rule for device length $L_{\text{dev}} \sim 3L_c^0$ also means a device length

$$L_{\text{dev}} \sim 3L_c^0 \sim 3\pi L_d \ , \tag{3}$$

hence ~9.4 times the decay length *at the critical point*. Note that Fig. 1(a) is universal (it could be made dimensionless). The factor 3 looks somewhat arbitrary, but referring to Fig. 1(a), we see that we are exploiting the SEB in the region where, for the imaginary eigenvalues, the parabola local slope is a few times larger than their asymptotic $\pm \frac{1}{2}$ slope.

Let us now turn to the application where plasmonic waveguides are used as the loss material. Needless to say, metallic losses at visible or near-infrared frequencies cannot be tuned, so we have to do with fixed losses, *in one of the channels*. But it is perfectly possible to imagine an architecture with only the variable gain g_1 still in WG1, and fixed losses, - g_0, in WG2.

This breaks the rule $\varepsilon_{(-x)} = \varepsilon_{(x)}^*$ except if gain is matched to fixed losses (and again, it mostly suffices that waveguide eigenvalues work as described below, because a guided mode "picks up" amplitude in a singular way, ignoring the detail of the field map. For instance the guides can be of completely different nature). Without any precaution, a pattern reminiscent of Fig. 1(a) arises when we solve for the eigenvalues of the evolution with a fixed loss.

$$i\frac{d}{dz}\begin{pmatrix}\psi_1\\\psi_2\end{pmatrix}=\begin{pmatrix}\beta_1+ig_1/2 & \kappa\\ \kappa & \beta_1-ig_0/2\end{pmatrix}\begin{pmatrix}\psi_1\\\psi_2\end{pmatrix} \qquad (4)$$

However, by analogy with the former critical point situation $\kappa = g_1^{\text{crit}}/2$, we find that if we match coupling to fixed losses of WG2,

$$\kappa = g_0/2, \qquad (5)$$

we may restore the essence of the SEB behaviour, as shown in Fig. 1(b), where the abscissa is still the WG1 variable gain g_1. The real part of the propagation eigenvalues (the wave-vectors) now follows, from zero gain to the critical point, a slightly modified parabolic trend and the imaginary part grows linearly from overall loss to zero loss. At the critical point, both the real and imaginary parts are equal to zero as in the canonical case of Fig. 1(a). This behavior arises because we have followed the prescription given by Eq. (5); in general, it is not possible to center the critical point around zero unless this condition is satisfied. Above the critical point, the real parts are zero as in the canonical case while the parabolic divergence of the imaginary parts is similar to the curves of Fig. 1(a). When the gain further increases, the negative imaginary wavevector (the decay constant) of one mode levels off to the plasmonics level – $g_0/2$ while the other grows linearly. Hence the heart of the SEB behaviour still holds, notably the SEB with opposite signs of imaginary parts.

The feasibility of matching losses and coupling [i.e., Eq. (5)] is hardly questionable, it only amounts to approach one guide at the adequate distance from the other, a distance that can be made compatible with current technology [15]. We will discuss later in Sec. III the specific cases of coupled waveguides using LRSPP as the plasmonic guide, or using the PIROW waveguide.

We can finally compare Fig. 1(c) to Fig. 1(d), the map of $T_{11}(g_1)$ vs. gain and guide length occuring for the situation of Fig. 1(b): no major difference can be seen as regards the SEB critical region in the center. But in the large gain region on the right, there is of course a difference, and even more markedly in the lower left low-gain region and long length, since the remaining losses increasingly attenuates light in both WGs in this case. The relative difference is also marked if one draws a similar map of $T_{21}(g_1)$ that addresses the exit of the lossy channel (not shown) because the negative imaginary eigenvalue levels off in the present case instead of steadily decreasing in the canonical case.

A first simple step to test the validity of coupled mode theory (CMT) can be made with a pair of coupled slab waveguides with weak index steps similar to those that will be used on the dielectric side of the LRSPP solution below, stemming here from the use of the familiar resists SU8 (n = 1.57) and BCB (n = 1.535) in the infrared. Using a finite element mode solver, we checked that both real and imaginary parts were in line with the CMT prediction for matched gained or fixed gain (Fig. 3 shows the imaginary parts in both cases, and the caption provides the relation of bulk imaginary constant to modal constant). The agreement in this one-dimensional case is very good. A very small discrepancy in the fixed loss case, typically a few 10^{-5} in ordinate, shown by diamonds with $\times 100$ magnification, is thought to

stem from the dispersion of the real part induced by the gain, not affecting sizably the transmission behavior.
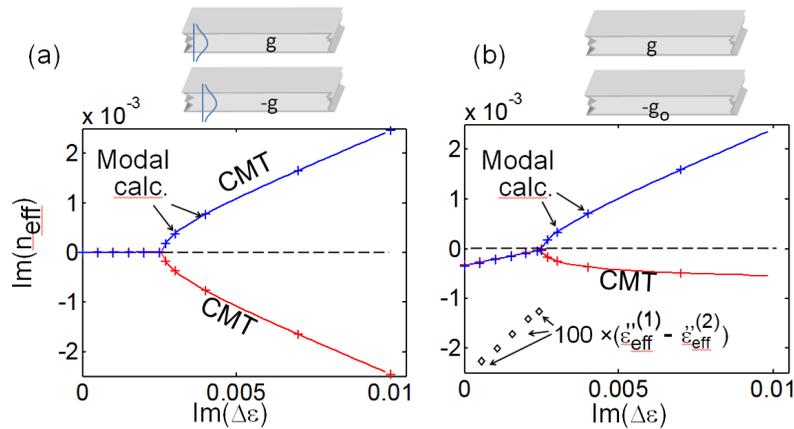

Fig. 3. Comparison of CMT results (solid lines) with two-slabs finite element calculations (crosses) (a) case of symmetric gain and losses; (b) case of fixed losses. The parameters are: thicknesses of 2 µm, inner separation 2.5 µm. Dielectric constants are $1.57^2 \pm \mathrm{Im}(\Delta\varepsilon)$ in the core (SU8 typical value) and 1.535^2 for the cladding (BCB refractive index). $\mathrm{Im}(\Delta\varepsilon) = 0.01$ corresponds to 206 cm^{-1} modal gain of a single guide. The minute difference between imaginary eigenvalues in (b) before critical point is magnified hundred times (diamonds).

To conclude this section, we found that there is a clear margin for device operation with an imperfect PT system, namely with fixed losses (and even with waveguides of different nature). Recently, waveguides with metallic losses coupled to passive dielectric waveguides have been considered in order to form so-called "passive-PT-structures" [20,21]. Physical features such as inverse loss dependence of the output field were shown to occur at loss levels lower than the PT-symmetry breaking. However these studies do not address our point that the SEB could be restored so as to display properties similar to ideal PT symmetric devices, explicitly targeting the singular region to get enhanced modulation capabilities. The modulation in a passive PT structure can offer a nonintuitive output passing through a zero and returning to unity when loss increase, but it results from the varying coupling length that stems from the decreasing eigenvalue splitting, similar to the left part of Fig. 1(a) and it does not exploit the SEB region itself, and could not do so because this very region suffers from high losses in this configuration.

For the system considered in the present paper, we gave a design rule $\kappa = g_0/2$, Eq. (5), leading to a desirable device length $L_{\mathrm{dev}} \sim 3L_c^0 \sim 3\pi L_d$ exactly as in Eq. (3) and for the same reasons. Although we postpone a tolerance study, we do not foresee much surprise in the targeted switching mode of operation. As for gain, while it was a formal parameter in the above, we shall detail below what can be designed on the one hand and what amounts of material gain are realistic in the visible on the other hand.

We can add for the time being that the behaviour inferred could be realized not only by having a single waveguide WG1 with gain swept from zero to on, but also by a combination of two gain means, such that a "baseline" gain is implemented in quasi cw mode by one of these means, while the switching operation is ensured by a smaller control gain induced by the other mean. For instance, a layer of waveguide WG1 can be optically pumped by a control optical signal for approaching the critical/switching point, while an electrode provides extra gain into another layer, or vice versa. Tightly coupled ridges can also serve such a purpose. Hence there is a lot of room for the architecture on the gain side. But since this is not an established technology, not as much as e.g., gain in GaAs- or InP-based semiconductors in the infrared, we shall devote a section (Sec.IV) to clarify why organic gain materials can be ideal

candidates for a proof of principle and give a brief survey of gain in organics with a device perspective. Its main scope will be to assess the length scale of targeted PT-symmetric devices through the range of gain values that can be attained. We will justify that gains on the order of 100-500 cm^{-1}, while not commonly assessed nowadays in organics, could nevertheless be targeted. But prior to this final section, in the following Sec.III, we detail the coupled waveguide architectures in the two specific cases of LRSPP waveguides and PIROW waveguides, using the trends from the theoretical analysis.

3. Coupled waveguides in plasmonics and SEB device architectures

3.1 Plasmonic waveguiding

Plasmonic waveguiding (using extended plasmons as opposed to localised ones) was set on firm basis by Berini's work [22,23] (needless to say, 2D surface plasmons are documented in textbooks and many reviews). If we restrict ourselves to 1D channel waveguiding, the state-of-the-art has gone well beyond the basic rectangular geometry cited above. For instance, extensive reports concern metallic V-grooves to propagate with reduced losses or wedges [24–26]. Generally speaking, many of the building-blocks of integrated optics have been transferred to SPPs with success (bends, Bragg gratings, focussing elements etc.) [27]. Hybrid waveguiding [14,18] is one of the best solutions to retain strong confinement, while LRSPP reduce losses by thinning the gold or silver layer to a point where strong deconfinement occurs [3,25,28]. A theoretical and experimental account of plasmonics systems with a gain-carrying dielectric layer can be found in [29].

Plasmonic and dielectric waveguides can be coupled among themselves or in combination. For instance [30] reports on coupling between silicon and copper plasmonic nanoslot waveguides in the framework of MOS technology. A recent illustration of a less confined case was reported by Ref. [31] whereby a LRSPP waveguide similar to those of [4] and [3] was coupled to a polymer one.

3.2 Device with long-range plasmonic waveguide (LRSPP)

The simplest target to implement SEB is the coupled LRSPP and dielectric case. For the parameters of [31], i.e. a wavelength of 1.55 µm, an elongated Au cross section of 36 nm × 4,6 µm, a dielectric waveguide made of SU8 (refractive index n ≈1.57) having about a 1.5 × 2 µm^2 cross section, a typical coupling length of $L_c^0 = 400$ µm was found. The decay length $L_d = g_0^{-1} = \lambda / 4\pi |\mathrm{Im}(n_{\mathrm{eff}})|$ of the LRSPP, however, is as long as ~4 mm ($|\mathrm{Im}(n_{\mathrm{eff}})| = 3\ 10^{-5}$ at $\lambda = 1.5\ \mu m$). A typical profile of the two split modes of transverse magnetic polarization is given in Fig. 4.

We have calculated this case in more detail following our prescription to get imaginary eigenvalues singularity near zero. We have used various commercial or specialized mode solvers, and mainly COMSOL which provided well converged results when fed with adequate initial guesses. The results retain most of the expected features even though additional effects that were not present in the one-dimensional case makes the desired adjustment of coupling that brings the SEB at zero imaginary eigenvalues less straightforward than in the model case.

Hence, our studies of eigenvalues assess the viability of the main ingredient of the present plasmonics + PT-symmetric approach in a realistic case.

We can now discuss the overall device working point in practical cases, in order to operate the device around the SEB with increased modulation using the expressions based on length: $L_c^0 = \pi L_d$ (with $L_d = g_0^{-1}$) and $L_{\mathrm{dev}} \approx 3L_c^0 \approx 3\pi L_d$. Data will be gathered in Table 1.
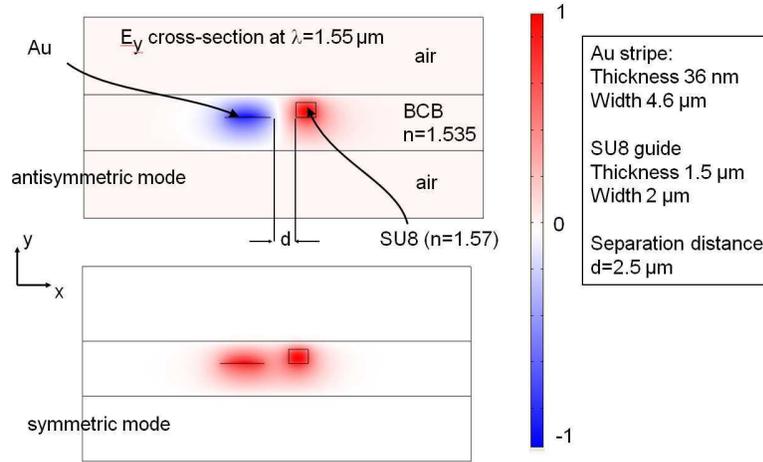
Fig. 4. LRSPP + dielectric waveguide based on SU8 and gold in BCB. Color map of y electric field component for antisymmetric and symmetric modes.

In the present case, we find two approaches: either, from the basis of $L_d = g_0^{-1} = 4$ mm decay length, the coupling length has to be stretched to the very large value of $L_c^0 = \pi g_0^{-1} \sim 13$ mm and L_{dev} is in the 40 mm range, or we decide to operate at larger losses to fit for instance a much smaller coupling length $L_c^0 = 400$ µm with a much shorter LRSPP decay length $L_d = L_c^0 / \pi = g_0^{-1} = 127$ µm. The former case requires simply a larger spacing, typically 5 µm to 7 µm. The latter case requires a thicker gold layer (in a well mastered range), and a more confined mode, thus a closer proximity of the LRSPP and dielectric waveguides, typically around 1.0 to 1.5 µm. Let us continue the dimensioning in this less hypothetical second case; then a modal gain of 80 cm^{-1} is required, well in the range of mastered gains. This can further be translated in terms of bulk gain. The typical confinement factor of the SU8 waveguide for the magnetic modes of interest is about $\Gamma = 0.9$. Therefore, a bulk gain of about 90 cm^{-1} is needed. In practice, one would first qualify a broad SU8 test film with the same thickness (1.5 µm) as the waveguide, targeting nearly the same modal gain, since presence or absence of the in-plane confinement affects Γ to less than 10%. The overall device cross-section for this assumption of stronger losses, will be essentially limited by the dielectric guide one, the LRSPP being, after this modification, smaller than the dielectric one.

These figures can now be interpreted in terms of gain enhancement from the SEB effect, also collated in Table 1: As discussed before, a typical modulation of the gain that would ensure a switching requires about 20% modal gain variation, or 15-20 cm^{-1} in the design with $L_c^0 = 400$ µm. Recalling [cf. Fig. 1(d)], that we do not operate at the zero-gain coupling length $L = L_c^0$, but around $L_{dev} = 3L_c^0$, a LRSPP-based realization exploiting the geometry proposed by [31] ($L_c^0 = 400$ µm) would eventually demand $L_{dev} = 1200$ µm to operate as a gain-enhanced switch. Still, because the switching limits correspond to $T_{11}(g_1) = 0$ and $T_{11}(g_1) \sim 10$, the result is appreciable in the sense that a contrast C = max($T_{11}(g_1)$)/min($T_{11}(g_1)$) that can reasonably be hoped to exceed C > 200 is obtained from a small modulation, associated with $\Delta g \, L_{dev} \approx 2.5$. Thus, the inequality exp($\Delta g \, L_{dev}$) $\approx 10 \ll 200$ manifests the interest of the result.

For a still shorter design, $L_{dev} = 3L_c^0 = 400$ µm, we have to correct again the gain data by a factor 3.0, targeting a 240 cm^{-1} modal gain (see Sec.IV) and a 50-60 cm^{-1} gain modulation. The ~40 µm decay length is now shorter than those typical of LRSPP at 1.5 µm, one should recourse to shorter range SPP or to plasmonics systems other than gold, e.g., based on Aluminum. We let the details of this exercise to a later work.

Another variant is to explicitly switch from infrared to a visible wavelength to get higher losses in the privileged case of gold. Going to the visible wavelength would shrink both LRSPP and dielectric waveguides with an obvious scaling as regards transverse dimensions of the dielectric given the constant index contrast, and a more refined scaling for the metal given the detailed metal dispersion. The above scaling exercise would now bring us to attempt a design at $L_{dev} = 3L_c^0 = 190$ µm and losses (decay length) of -500 cm^{-1} (20 µm), which falls in the typical range of red/near infrared ordinary surface plasmons. Note that once the losses are set to a given value, our discussion on gain and gain-modulation advantage is unchanged in absolute terms.

Table 1. Basic Designs of PT-Symmetric Devices for LRSPP-Based Waveguides in the Infrared or in the Visible, and for PIROW-Based Waveguides

Design	LRSPP			LRSPP	PIROW
	LRSPP and SU8[a]	*Loss-matched design*	*Short Design*	*Visible wavelength design*	*Au or Ag + high index*
Wavelength (nm)	1550	1550	1550	700-800	633
SEB-Coupling length at zero gain (µm)	13 000	400	133	62	62
Device length (µm)	39 000	1200	400	190	190
Losses $-g_o$ (cm^{-1})	−2.5	−80	−240	−500	−500
Baseline gain (cm^{-1})	**2.5**	**80**	**240**	**500**	**500**
Gain modulation (cm^{-1})	**0.5-0.6**	**15-20**	**50-60**	**80-120**	**80-120**
Dielectric waveguide section µm × µm	1.5 × 2.0	1.5 × 2.0	1.5 × 2.0	~0.7 × 0.9	(See Fig. 5)
LRSPP data µm × µm	4.6 × 0.036 (Au)	4.0 × 0.1 (Au)	see text	Simple surface plasmon	See text
Separation (µm)	2.3	1.5 ?	1.0 ?	~1.0	0.9

[a]From New J. Phys. **11**, 015002 (2009) [31].

3.3 Device with hybrid PIROW waveguide

To address more miniature devices, it is necessary to confine the optical mode with the help of the metal, but to keep losses under a reasonable maximum. Therefore, dielectrics should also be used to assist guidance and relieve the higher losses incurred by standard plasmonics confinement. In the case of our PIROW waveguide [18], gold layers operated in the red part of the spectrum, where organics are easily available, were suggested. Typical decay length figures for such waveguides are in the 5-10 µm range. We can therefore seek coupling length of the same order for a SEB-effect design.

Since there are no clearly privileged strategies to couple a gain-carrying dielectric waveguide to a hybrid waveguide [15], we prefer to pave the way to such architectures by studying the case of a double hybrid (PIROW) waveguide [18], indeed closer to Fig. 1 in essence. The basic layout of a single PIROW is sketched in Fig. 5. It consists of a flat metallic sheet, retaining the best metal properties and minimal edge roughness, topped by a low-index

material in which a trench has been made, which has been used to directly define an inverse-rib high index structure, e.g. by spin-coating a relatively high-index material (sol-gel or organic). To retain a high degree of confinement a very thin region of thickness b made of low-index material is preserved between the inverse-ridge bottom and the metal, much as the magnesium fluoride layer in [2]. The electric field of the quasi-TM mode peaks in this region, which favors a number of photonic figures of merit such as the Purcell factor, with a mechanism reminiscent of the slot-waveguide physics.
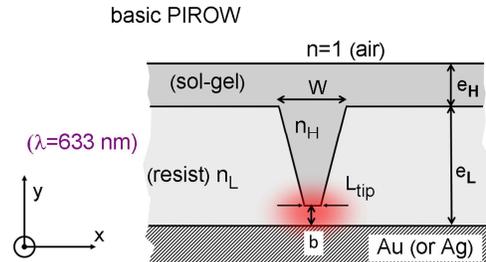

Fig. 5. Sketch of the PIROW cross-section: an inverse-rib of high-index material coats the grooved low-index material. It can be obtained by spin-coating for instance. The field concentration at the tip end makes the details of the top side relatively unimportant.

Let us first insist that a *single* genuine hybrid waveguide itself cannot be modeled as a set of a coupled dielectric and plasmonic waveguides supporting a combination of their individual modes: the eigenmodes are way too different, the field profile of a genuine hybrid waveguide is concentrated between the metallic and high-dielectric regions, decaying not only in the metal but also *inside* the high dielectric region, whereas the field profile, in a situation of weakly coupled modes, only decays *outside* the high-dielectric region. When approaching a high-index waveguide from a metallic one, looking at the properties as a function of physical separation, there is thus a transition domain across which the coupled mode picture loses its sense.

We mostly need to study the coupling of two PIROW waveguides to arrive at a first-order design. Using the same finite-element code as in [18], but symmetrizing the domain from x>0 to x<0, we get eigenmodes with both parities with respect to the central mirror plane.

In Fig. 6, we show the dispersion of the two split modes of a pair of PIROW waveguide separated by a variable distance d. Parameters of materials are indices n = 2.0 (high index, inverse rib), 1.5 (cladding) and a standard tabulated refractive index for gold. The insets on the sides show the symmetric and antisymmetric modes for both cases, not showing much actual difference, implying that they experience a strong "pinning" effect of the inverse-rib narrow gap structures. The overall trend of index difference of the supermode is dictated by the lateral decay length of individual modes. The fact that the lower supermode effective index goes through a maximum is probably originating from the still favourable effect of adding higher dielectric material when forming the second waveguide rather than making a balanced perturbation to the original single guide situation (one could for instance move high dielectric from one place to another in the mode profile, for instance).

We can now design the device by imposing its length $L_{\text{dev}} = 3L_c^0$ first, say again $L_{\text{dev}} = 190$ µm, ($L_c^0 = 62$ µm coupling length), hence we target $500\,cm^{-1}$ modal gain (the physical gain region could be limited to the sole inverse-rib, for instance, to pump a small volume, see below). This is still a value that compares to the likely modal gain of surface plasmon lasers [2]. The coupling length of 62 µm is also associated with a splitting of the real eigenvalues such that $L_c^0 \Delta n_{\text{eff}} = \lambda / 2$ (supermodes are out of phase), hence we need to locate on Fig. 6 the

separation between two PIROWs such that $\Delta\operatorname{Re}(n_{\mathrm{eff}}) = \lambda/2L_c^0$. For a wavelength of 620 nm, this points toward $\Delta\operatorname{Re}(n_{\mathrm{eff}}) = 0.005$ only, hence a separation d of nearly 0.9 µm.
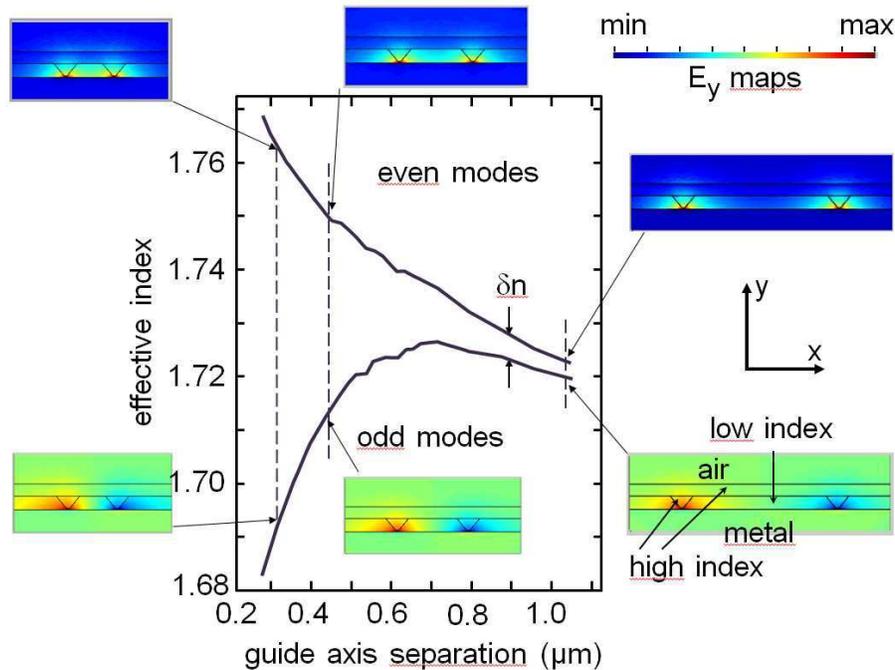

Fig. 6. Effective indices of the two split-mode of two coupled PIROWs as a function of distance of separation d. The system has no gain, only losses, on the order of $\left|\operatorname{Im}(n_{eff})\right| = 0.0123$ for both supermodes typically. The point with $\left|\Delta\operatorname{Re}(n_{eff})\right| = 0.005$ at $d{\sim}0.9$ µm is indicated by the arrows.

But for the exact losses, here with gold, this particular PIROW design results in $\left|\operatorname{Im}(n_{\mathrm{eff}})\right|$ = 1.25 10^{-2} (nearly the same value for a single mode or a supermode), thus we have $L_d = g_0^{-1} = \lambda/4\pi\left|\operatorname{Im}(n_{\mathrm{eff}})\right| \sim 4$ µm, about $-g_0 = -2500$ cm^{-1}, fivefold our target modal gain. Thus for the next iteration, we are faced to two possible choices, much as was seen for LRSPP: (i) going to smaller coupling length and device size, here about $L_{\mathrm{dev}} = 70$ µm, which is a miniature solution, but difficult in terms of gain; (ii) the other solution is to reduce losses by either going to the more infrared wavelength range, beyond 660 nm, to nearly halve the absorption of gold, which would already bring us to the -1300 cm^{-1} range and then to finely adjust the gap/rib profiles to optimize the loss figure to the target (-500 cm^{-1}) . We assume that gain will be mostly lying in the high index medium, so the modal distribution will dictate the relationship between material gain and modal gain, as hinted for slab waveguides. A broader inverse-rib and/or a less steep angle will localize the mode, keeping a large enough coupling length, and it will allow material gain to maximally participate to the modal gain. So we anticipate that the design window is a target modal gain 500-1000 cm^{-1}, and a device length 200-400 µm, for a separation of 0.9-1.2 µm. Anyway, this is only the first coupled hybrid waveguide calculation for PIROW. Much work remains to be done to check what indices will be best implemented in PIROWs, and which materials bring the highest gain opportunities. In the next section, we review the possible organic gain devices that could be implemented for the gain branch of our SEB devices.

4. Organics gain in layered devices

Organic pi-conjugated systems are good candidates for providing gain in plasmonic PT symmetric devices, not only because they comply with the high gain requirements, but also because they can be processed easily with various techniques (from solution, or thermally evaporated) which makes them ideal choices at least for early proof-of-principle developments. Noginov spaser [16] used an organic dye-doped silica shell surrounding a gold nanoparticle, for instance. Furthermore, organic materials, i.e. classical laser dyes and organic semiconductors, are boosted by the rapid growth of Organic Light Emitting Diode and organic photovoltaic devices. Although an electrically-pumped organic semiconductor laser diode has not been yet demonstrated [32], the possible opportunity to electrically drive organic systems would be an additional benefit towards higher integration and lower costs for plasmonic devices.
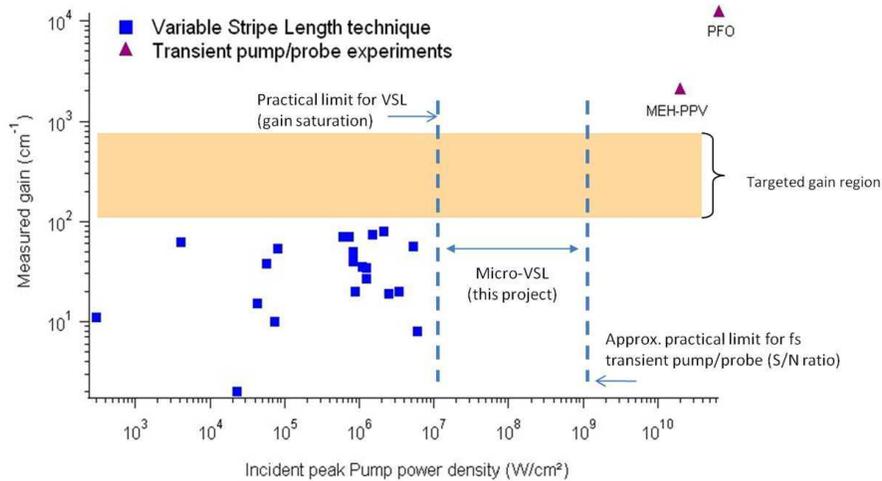

Fig. 7. Measured gain as a function of incident peak power for various literature results corresponding to different methods as indicated.

There is curiously no clear agreement on the gain values that can be achieved with organic films (see Fig. 7), firstly because many materials still unpredictably suffer from ambient conditions (oxygen, moist) and/or from quenching and bleaching, and secondly because the classical paradigm for an operational organic laser is a "low loss" cavity (with good mirrors, Distributed Bragg Reflector, DBR or photonic crystal) which puts the gain material in a position to work in a low gain regime. Plasmonics push organics to a quite unexplored domain where they are required to work as high-gain materials in high-loss environments. Candidates are either (i) dyes such as Rhodamine dispersed in polymeric resists or sol-gel hybrids or (ii) organic semiconductors, which in contrast to dyes are able to emit under the form of neat undiluted films: they may be conjugated polymers such as PPV derivatives or MeLPPP [33] or molecular films of amorphous small molecules [34].

Literature on gain measurements in thin films of organic media is abundant but paradoxically no trend can be drafted about the compared merits of different gain materials, since both materials and experimental conditions strongly differ from a report to another. Defining a simple figure of merit is complex: basic spectroscopic data such as stimulated emission cross section (σ) are not sufficient to rank a material as photogenerated states (triplets, polarons, etc.) and quenching intervenes in a complex fashion in the total population inversion that can be reached, directly impacting the achievable gain.

The question here is then to know whether gains in the targeted zone (roughly between 10^2 and 10^3 cm^{-1}) are achievable in organic waveguides. Very high gains have been reported in

organic semiconductors with femtosecond transient pump-probe experiments (see Fig. 7): Wegmann *et al*. [35] obtained 2000 cm^{-1} in MeLPPP at a 400 fs delay after excitation, and Virgili *et al*. [36] claimed 12 000 cm^{-1} in a film of Polyfluorene at $t = 0$ fs delay. These gains are derived from a change in the transmission of the sample; they are given at a specific time t and represent a "local gain" (product of emission cross section by local population inversion), not directly the waveguide modal gain, which can be thought as a spatial and temporal average of local gain. A similar technique (with a pulsed ns pump and a cw probe) was used by [29] in a plasmonic waveguide (in a Kraetschmann-Raether configuration) yielding a gain of 420 cm^{-1} in a PMMA film doped with Rhodamine 6G; this value, deduced from a reflectivity measurement, is still not a direct measurement of gain.

The most direct and widely used technique to measure waveguide gains is the so-called "Variable stripe length" (VSL) technique [37]. It does not require the injection of a probe beam by the film edge, which may be problematic in organic films where edges are never well-defined. The technique consists in exciting the material from the top by a pump beam tailored under the form of a thin stripe of variable length and monitoring side-emitted Amplified Spontaneous Emission (ASE). The gain g (in cm^{-1}) is deduced from the ASE intensity I dependence versus pump stripe length L by a simple formula, which holds in a 1-D approximation and whenever gain saturation is negligible:

$$I(L) = \frac{\eta_{\text{spont}}}{g - \alpha} \Big[e^{(g-\alpha)L} - 1 \Big] \tag{6}$$

where α represents the passive losses (self-reabsorption and waveguide losses), η_{spont} is the power density of spontaneous emission emitted into the stripe equivalent solid angle (fraction of spontaneous emission, akin to the so-called β-factor).

The VSL technique has been used in thin crystal slabs, organic films, QD, and recently silicon nanocrystals [38], but is often poorly practiced because large deviations from the assumptions subtending Eq. (6) easily arise, either in coherent optics on the excitation sides, or due to the breakdown of the quasi-1D approximation [39]. It is however possible to improve the accuracy of the measured gain through a careful design of the optical system: by imaging a couple of razor blades instead of placing the sample at a fixed distance from them, the customary Fresnel diffraction pattern of excitation beam is virtually eliminated and a sharp profile is defined for the pump stripe, thus eliminating the need of a complex algorithm to retrieve the gain [34]. Modeling efforts can also be done to take into account gain saturation issues [40].

A rapid analysis of the published gain measurements with the VSL method (Fig. 7) shows that the reported gains all cluster in the range 10^0-10^2 cm^{-1}, although pump energies/peak powers vary across several orders of magnitude and materials may be totally different. It is important to notice that this *apparent upper limit* of $\sim 10^2$ cm^{-1} is *a practical limit*: when stripes (typically ~ 100 µm wide, allowing a very small divergence of ASE) are formed onto the sample, a gain > 100 cm^{-1} is inevitably associated to a low saturation intensity, which is readily attained within less than 1 mm as far as the guided mode is confined (even loosely). This means that the *I(L)* dependence strongly departs from Eq. (6) after only a few hundreds of µm of propagation, invalidating the 1D approximation considering that ASE is directional. For these reasons, it is generally preferred to lower the pump intensity to obtain reliable data over several mm of propagation. There is therefore no fundamental difficulty hindering the measurement of higher gains, provided that the pump stripe is made thinner and higher pump fluences are used. Photodegradation will ultimately limit the affordable pump fluence, but there is still a comfortable margin before attaining a regime where device lifetimes become too short to be practicable. The peak intensities used in Refs. [35,36] are indeed of the order of 10^{10} W/cm^2 while intensities used for VSL measurements typically range from 10^3 to 10^6 W/cm^2 [41,42].

To illustrate this aspect, we measured the gain in a well-established system, a 20-µm thick PMMA layer doped with Rhodamine 640 (1 wt.%): with pump power density of 5.10^5 W/cm^2, a net gain of 35 cm^{-1} was obtained by the VSL technique. In the meantime we realized a Vertical External-Cavity Surface-emitting Organic Laser (VECSOL) with the same material excited at a power density above 10^7 W/cm^2 [40] and observed device lifetimes under these conditions to be still > 5000 pulses under ambient conditions. This would mean that if gain was just proportional to pump fluence, gains on the order of 700 cm^{-1} should be expected with a good lifetime. Bleaching and excited-state interactions probably lower this value to some extent, but it demonstrates that the targeted zone (100 cm^{-1} < g < 500 cm^{-1}) for confined plasmonics cases such as the PIROW is within reach. It is an important point as it directly determines the size of active devices and the degree of miniaturization of this SEB plasmonics approach.

Therefore, not only the architecture of a device exhibiting SEB has to be done according to the design rule of Sec.II, but also the way to implement gain assessment has to be done in such a way that higher gains can be measured, up to 500 cm^{-1} typically, notably through an improved VSL setup. It has to be noticed that these high gains favor the emergence of amplified stimulated emission that will tend to cause gain saturation, which does not affect the expected behavior around the critical point as already pointed out. From the experimentalist point of view, high gains may also favor unwanted lasing between weakly reflective contacts or scattering defects (random lasing), adding potential technical difficulties but not affecting the fundamentals of SEB.

5. Conclusion

Following the demonstrations that the properties of some non Hermitian systems with PT symmetry behave either with real or complex eigenvalues, we have attempted to tackle this issue to elaborate novel PT devices based on plasmonics. Although plasmonic waveguides have fixed losses that cannot be matched to the varying gain of the system, we offered a design rule that preserves the critical behaviour at the transition between real and imaginary eigenvalues: the coupling constant should be matched to the fixed losses.

We have next discussed two possible implementations of such systems: the first one targets low gain, and correspondingly makes use of a LRSPP waveguide as a loss channel. We have shown that a design operating in the 400 µm range even at 1550 nm requires much larger coupling and losses than the realisation in [31], and this is indeed favourable to miniaturization. This is of course even clearer if a visible radiation design is considered. Thus "compact" LRSPP systems could be privileged in this approach. The second implementation is based on the PIROW waveguide recently proposed, operating at much larger losses and targeting device size in the 100-200 µm range.

We have finally assessed whether the current organic gain system could be implemented as well to ensure gain of a higher order of magnitude than commonly assessed, by remarking that this assessment heavily rests on the sole VLS method, a situation that likely limit the obtainment of a large gain measurement anyway. We have hinted at good reasons to invoke gain values up to 500-1000 cm^{-1} in robust enough systems for future integrated photonic circuits.